# Quantum properties of irrational triangular billiards

F. M. de Aguiar
*Departamento de Física, Universidade Federal de Pernambuco, Recife, PE 50670-901, Brazil*
(Received 15 June 2007; revised manuscript received 21 December 2007; published 4 March 2008)

Triangles with sides given by consecutive integers ($N$, $N+1$, $N+2$) are fully irrational (all angles irrational with $\pi$) if $3<N<\infty$. Rational approximations to their angles and the Hurwitz theorem in number theory are used to define a parameter $h$ that quantifies the irrationality of each triangle. The energy level statistics [spacing distribution $p(s)$ and spectral rigidity $\Delta_3(L)$] of quantum billiards from this one-parameter family of triangles are investigated. The behavior of $h$ with varying $N$ and the numerically calculated level dynamics are found to be closely related: $h$ exhibits a local maximum at $N=10$, around which agreement with Gaussian orthogonal ensemble (GOE) spectral fluctuations is observed. As $N$ is increased, $h$ decreases and the statistics depart from GOE. Structures appear in $p(s)$ for $N>120$ and eventually the occurrence of gaps in the distribution for $N \sim 180$ define the onset of a long crossover towards the sequence observed in the integrable limit of the equilateral triangle ($N\rightarrow\infty$).

DOI: 10.1103/PhysRevE.77.036201 PACS number(s): 05.45.Mt, 05.45.Pq

## I. INTRODUCTION

Billiards are mathematical models used to describe the classical dynamics of Hamiltonian systems they are isomorphic to. In a billiard, one considers the motion of a point particle that moves uniformly between specular reflections at fixed scattering obstacles in a bounded domain. The resulting dynamics may vary from completely regular to fully chaotic, depending on the geometry of the confining cell. Historically, billiard models may be traced back to the celebrated hard ball gases due to Boltzmann and Lorentz [1] in the early decades of statistical physics. By replacing the walls of the underlying container by periodic boundary conditions, and separating the motion of the center of mass, one may show that the dynamics of two hard balls can be reduced to a flow on a torus with a circular hole. Introduced by Sinai in the 1960s, this model underpins the modern ergodic theory of dynamical systems [1–3]. In the past two decades, both theoretical and experimental billiards enjoyed a great deal of attention and played a remarkable role in the search for elusive traces of chaos in quantum dynamics [4–8].

Nowadays, the dynamics of planar billiards of interest fall into one of three classes [3]: elliptic (convex billiards), hyperbolic (concave billiards), or parabolic (polygonal billiards). Here, we focus on a geometry that belongs to the latter class. Billiards in polygons are known to have zero metric [9] and topological [10] entropies. Thus, they are never classically chaotic. While they may be ergodic [11], "it remains unknown whether billiards in polygons can ever be mixing" [9]. That they are never mixing seems to echo in the mathematical community [9,12], despite contrary numerical evidences found in irrational triangles [13]. Motivated by this controversy, we have studied numerically the quantum properties of a family of fully irrational triangular billiards (ITBs), and the results are offered in this paper. Previously, numerical experiments [14] have related scarring [15] of some wave functions in quantum ITBs to periodic orbits that reside in a neighboring rational triangular billiard (RTB). Notice, however, that it is still an open problem whether every polygon has a periodic billiard trajectory [16]. Quantum RTBs have long been investigated in the physics community [17–21]. So is the case of triangles with at least one angle rational with $\pi$ [22–25]. Surprisingly, it seems that no systematic investigation of fully ITBs has been reported thus far. This work introduces a one-parameter family of ITBs that fills that gap.

## II. ONE-PARAMETER FAMILY OF FULLY IRRATIONAL TRIANGLES

The usual recipe for building triangular billiards is to assign rational or irrational values to the ratio between the inner angles of the polygon and $\pi$. Instead, we approach the problem by considering acute triangles with sides $N$, $N+1$, and $N+2$, where $N$ is an integer number. Thus, each triangle in the subset chosen may be labeled solely by the parameter $N$. As the lower limit, we have the Heron (area is also an integer) right triangle with $N=3$. The upper limit ($N\rightarrow\infty$) is the integrable equilateral triangle. In between ($3<N<\infty$), all triangles are fully irrational, as can be demonstrated by a theorem due to Varona [26], which states that, if $r$ is a rational number in [0,1], then $\pi^{-1}\arccos(\sqrt{r})$ is rational if and only if $r\in\{0,1/4,1/2,3/4,1\}$. Notice that these values correspond to the only angles from which one can build an integrable triangle. Some of the $N$-dependent angles are shown in Fig. 1. As an attempt to quantify their degrees of irrationality, we consider the Hurwitz's theorem in number theory: For every irrational number $I$ there are infinitely many rationals $p/q$ that approximate $I$ such that the error $E=|I-p/q|$ is less than the Hurwitz bound $M=1/(\sqrt{5}q^2)$. We use truncated continued fractions expansions to obtain a rational approximation to each angle. Let $r\equiv E/M$ for a given approximation. We look for $r$ values smaller than 1. Two different irrational numbers may have slightly different values of $r$ satisfying this condition ($r<1$), and we regard that with higher $q$ as a more irrational number. This criterion seems plausible if the irrational numbers are in [0,1]. We take that into account by defining the parameter $h\equiv rq$ as a measure of the irrationality of $I$. For a triangle in the one-

 

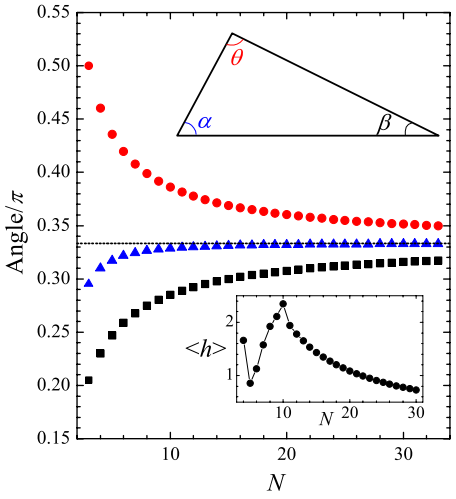


FIG. 1. (Color online) Inner angles of triangular billiards with sides ($N$, $N+1$, $N+2$), $\theta$(●), $\alpha$(▲), and $\beta$(■), as defined in the upper inset, divided by $\pi$. The horizontal line is the common asymptotical limit of 1/3. The lower inset is the calculated "irrationality", as described in the text.

parameter family above, we take the average of the values thus obtained for the three angles $\langle h \rangle$ as a measure of its irrationality. Some results are shown in the lower inset of Fig. 1: As mentioned previously, $\langle h \rangle$ exhibits a maximum for $N=10$ and smoothly drops as $N$ increases. A remarkable correspondence with this behavior is found in the level dynamics of quantum ITBs, as shown in the next section.

## III. SPECTRAL STATISTICS

Consider then the quantum dynamics of a particle bounded in one of these two-dimensional triangular wells. We solved numerically the underlying Helmholtz equation

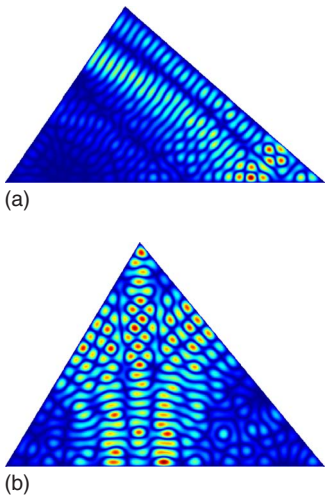


FIG. 2. (Color online) Density plots showing scarred wavefunctions in the $N=4$ (top) and $N=9$ (bottom) ITBs. They correspond to the 306th and 323rd eigenstates, respectively. Figures are not in the same length scale.

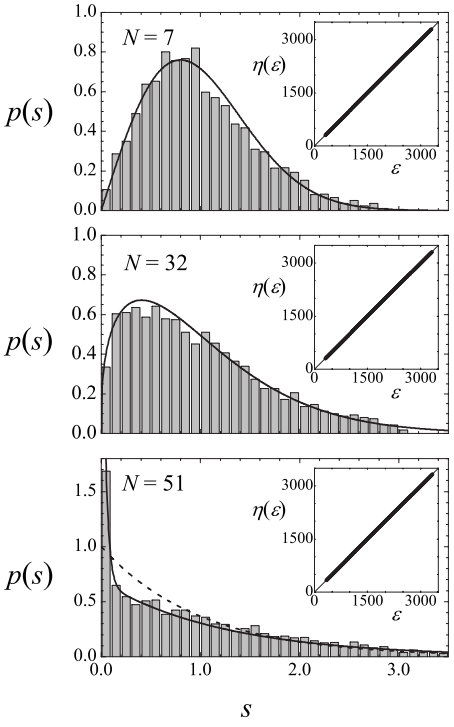


FIG. 3. Calculated nearest neighbor spacing distributions (histograms) for the ITBs with $N=7$, 32, and 51. Solid lines correspond to the Wigner (GOE) distribution (top), Brody distribution with $\nu=0.355$ (middle) and to the sum of two exponentials with different decay rates (bottom). The dashed line is the Poisson distribution. Insets show the corresponding staircase functions of the unfolded spectra (solid symbols) and the 45° line. The areas of the triangles are, respectively, $12\sqrt{5}$, $33\sqrt{3255}/4$, and 1170 ($N=51$ is a Heron triangle).

with a finite element method described elsewhere [27], that is satisfactory in regards to the experimentally accessible eigenvalues with microwave billiards [28]. Around 150 000 suitable triangular elements were used in the mesh for each triangle. Two scarred eigenfunctions are shown in Fig. 2 for $N=4$ and $N=9$. We have made no attempt to relate those states neither to periodic orbits nor to their "ghosts" [14], and just want to illustrate here possible quantum localization of eigenfunctions in ITBs. As for the statistical properties of the unfolded spectra, we considered sets of more than 3000 eigenvalues beyond the 300th level. Fig. 3 shows histograms for the nearest-neighbor level spacing distribution (NNLSD) for $N=7$, 32, and 51. The solid line in the top panel is the Wigner surmise for the Gaussian orthogonal ensemble (GOE) of random matrix theory (RMT) [29], showing a very good agreement for $N=7$. The solid line in the mid panel is a fit with a Brody distribution [Eq. (1) below] with $\nu=0.355$, and that in the bottom panel is a numerically normalized Poisson-like distribution given by the sum of two exponential decays with different rates, a fast one at small $s$ and a slow one at higher level spacing. The solid symbols in the insets show the staircase functions (number of eigenvalues less than or equal to a given value) of the unfolded spectra, which could hardly be distinguished from the unit-slope 45° solid lines, thus reflecting a good agreement with a Weyl-

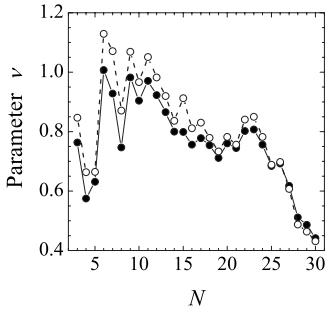


FIG. 4. Dependence of the Brody (solid circles) and Izrailev (open circles) parameters with $N$, in the level-repulsion regime. Lines are guides to the eyes.

type formula [4] and assuring the good precision of the data as well. In Fig. 4 we show both Brody and Izrailev $\nu$ parameters as functions of $N$. The phenomenological Brody parameter $\nu$ is obtained from best fits of the calculated NNLSD with the function

$$p(s) = (\nu + 1)a_\nu s^\nu \exp(-a_\nu s^{\nu+1}), \tag{1}$$

where

$$a_\nu = \left[\Gamma\left(\frac{\nu+2}{\nu+1}\right)\right]^{\nu+1} \tag{2}$$

and $\Gamma$ is Euler's gamma function. Equation (1) reduces to the Poisson [Wigner (GOE)] distribution for $\nu=0$ ($\nu=1$). The three-parameter Izrailev ansatz is given by

$$p(s) = As^\nu \exp\left[-\frac{\pi^2}{16}\nu s^2 - \left(C - \frac{\nu}{2}\right)\frac{\pi}{2}s\right] \tag{3}$$

and must be normalized numerically. One may relate Izrailev's $\nu$ parameter to the degree of quantum localization of the wave functions in the spectrum. It is clear from Fig. 4 that for smaller values of $N$, where repulsion is observed in the highly excited energy levels, and the angles in Fig. 1 are widely dispersed, it is more likely to find localized states such as the ones in Fig. 2. Remarkably, the behavior of parameter $\nu$ with $N$ is qualitatively similar to that of the mean irrationality shown in the lower inset of Fig. 1. These short scale results are consistent with the long-range correlations. Here we consider the Dyson-Mehta spectral rigidity $\delta_3(L)$, which gives the least-squares deviation of the staircase function from the best fit to a straight line, in an interval of length $L$. The mean spectral rigidity for the GOE is related to the two-point correlation function

$$Y_2(r) = \left[\int_r^\infty s(x)dx\right]\frac{ds(r)}{dr} + [s(r)]^2, \tag{4}$$

where

$$s(r) = \frac{\sin(\pi r)}{\pi r}, \tag{5}$$

via

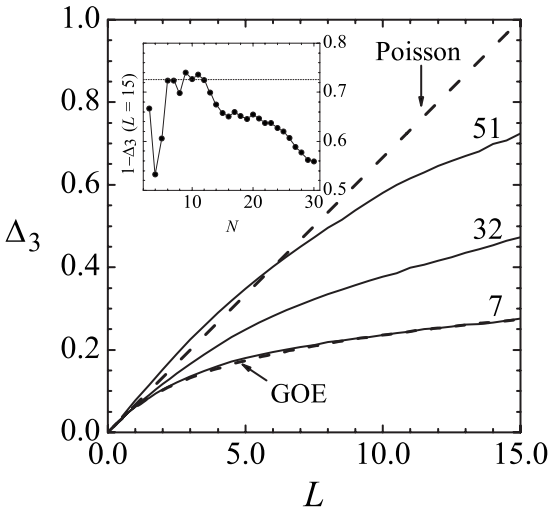


FIG. 5. Spectral rigidity $\Delta_3(L)$ for the triangles with $N=7$, 32 and 51 (solid lines). Dashed lines are for the GOE and Poisson statistics. The lines for the GOE process and for $N=7$ are almost coincident. Inset: $1-\Delta_3(L=15)$ as a function of $N$, showing the same trend towards the Poisson statistics as in Fig. 4. Dashed horizontal line is the GOE result. Solid line is a guide to the eyes.

$$\Delta_3(L) \equiv \langle \delta_3(L) \rangle = \frac{L}{15} - \frac{1}{15L^4}\int_0^L (L-r)^3(2L^2 - 9Lr - 3r^2)Y_2(r)dr, \tag{6}$$

whereas for a random sequence with no correlations (Poisson

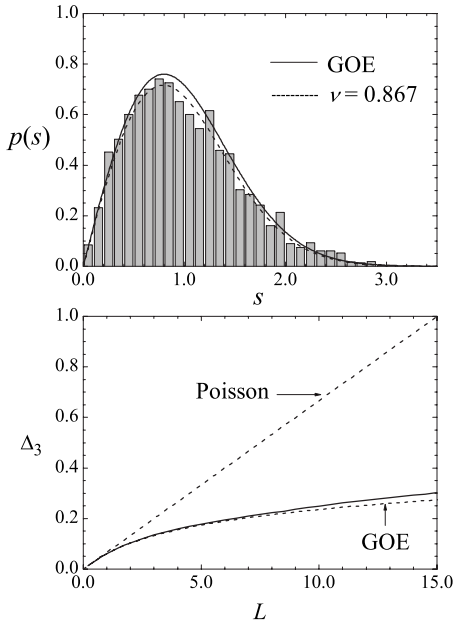


FIG. 6. Spacing distribution (top histogram) and spectral rigidity (solid line in the bottom panel), for an ITB previously studied by Casati and Prosen [30], as described in the text. The dashed line in the top panel is a best fit with Eq. (1) with $\nu=0.867$; the solid line is the Wigner distribution. The dashed lines in the bottom panel are for the Poisson and the GOE statistics.

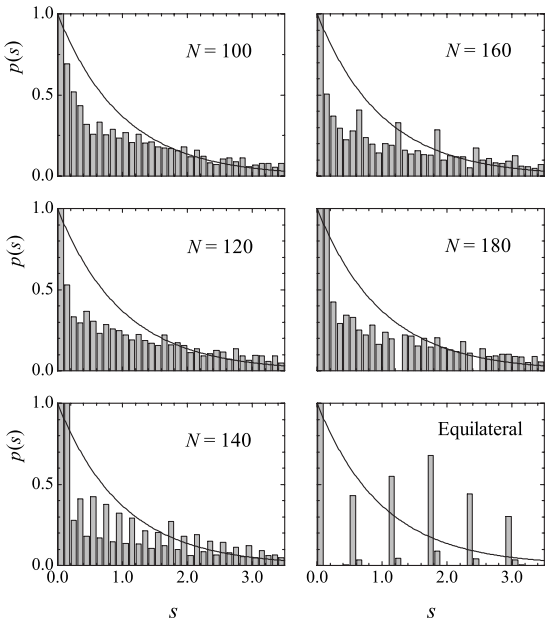


FIG. 7. Numerically calculated spacing distribution at the large-$N$ crossover regime and for the equilateral triangle. Solid line is the Poisson distribution.

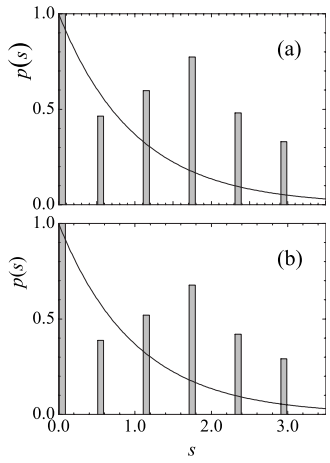


FIG. 8. (a) Spacing distribution of the equilateral triangle obtained from the 3000 eigenvalues beyond the first 300, calculated exactly. (b) Same as (a), for the 7000 eigenvalues beyond the first 3000.

process), we have $\Delta_3(L)=L/15$. The dashed lines in Fig. 5 represent $\Delta_3(L)$ for these two processes. The solid lines in Fig. 5 are the numerically calculated rigidities again for the triangles with $N=7$, 32, and 51, showing the same trend towards the Poisson statistic with increasing $N$, as the one shown in Fig. 3. The inset in Fig. 5 shows $f\equiv 1-\Delta_3(L=15)$ as a function of $N$, whose behavior might be compared to that shown in Fig. 4 and the lower inset of Fig. 1. For the Poisson process this function vanishes, whereas for the GOE process $f\sim 0.7262$. The latter is represented in the inset of Fig. 5 by the horizontal dashed line. The qualitative similarity between $f$ vs $N$, $\nu$ vs $N$, and $h$ vs $N$ is apparent.

## IV. DISCUSSION

Casati and Prosen [13] considered a fully irrational triangular billiard with angles $\alpha=(\sqrt{5}-1)\pi/4$, $\beta=(\sqrt{10}-1)\pi/8$, and $\theta=\pi-\alpha-\beta$. The corresponding ratios, $\alpha/\pi=0.309\cdots$, $\beta/\pi=0.270\cdots$, and $\theta/\pi=0.420\cdots$, geometrically place this triangle close to the ones in Fig. 1 with $N<12$. We have also calculated $p(s)$ and $\Delta_3$ for this billiard and the results are shown in Fig. 6. Confirming previous analysis by Casati and Prosen [30], a reasonable agreement with RMT is observed. However, the result presented here is evidence that this is not always observed in a fully irrational triangular billiard. A few words on the crossover towards a regime where the spectra might be approximated perturbatively from that of the equilateral triangle is in order. In Fig. 7 we show the numerically calculated $p(s)$ for $N=100$, 120, 140, 160, and 180, as well as that for an equilateral triangle, again for 3000 eigenvalues beyond the first 300. Periodic structures are observed in the distributions for $N>140$ and gaps are observed in $p(s)$ for $N=180$. The gaps become broader as $N$ increases and a characteristic sequence of the degenerate equilateral triangle is reached with $N\to\infty$, as shown in the right lower panel in Fig. 7. This is to be compared with the results obtained with the exact spectrum of the equilateral triangle, whose levels are given by $(m^2+n^2-mn)$, where $m$ and $n$ are integers such that $1\leq m\leq n/2$ [17,18]. All levels are degenerate, except those with $n=2m$. As in the numerical experiment of Fig. 7, the distribution in the upper panel of Fig. 8 was obtained with 3000 exact eigenvalues beyond the first 300, whereas for that in the lower panel of Fig. 8 we used 7000 *exact* eigenvalues beyond the first 3000. The similarity of the two distributions in Fig. 8 and the numerical one in Fig. 7 is indicative that our results in irrational triangular billiards are robust with respect to calculations at higher energies. It would certainly be of interest to test this robustness with other numerical methods [19,31]. Work in this regard is under way.

## ACKNOWLEDGMENTS

It is a pleasure to thank J. R. Rios Leite, A. M. S. Macêdo and R. Markarian for fruitful discussions and suggestions on the manuscript. The author is indebted to T. Prosen and G. Casati for making available unpublished results on quantum ITBs [30], and to W. R. de Oliveira Jr. for drawing Ref. [26] to his attention. Excellent assistance of D. D. de Menezes in the early stages of this work is gratefully acknowledged. This work is supported by the Brazilian agencies CNPq, CAPES and FACEPE.

[1] *Hard Ball Systems and the Lorentz Gas*, edited by D. Szász (Springer, Berlin, 2001).
[2] I. P. Cornfeld, S. V. Fomin, and Ya. Sinai, *Ergodic Theory* (Springer, Berlin, 1980); L. A. Bunimovich *et al.*, *Dynamical Systems, Ergodic Theory and Applications*, 2nd ed. (Springer, Berlin, 2000).
[3] E. Gutkin, Regular Chaotic Dyn. **8**, 1 (2003).
[4] M. C. Gutzwiller, *Chaos in Classical and Quantum Mechanics* (Springer-Verlag, New York, 1990).
[5] A. M. Ozorio de Almeida, *Hamiltonian Systems: Chaos and Quantization* (Cambridge University Press, Cambridge, 1990).
[6] F. Haake, *Quantum Signatures of Chaos*, 2nd ed. (Springer, Berlin, 2001).
[7] L. E. Reichl, *The Transition to Chaos*, 2nd ed. (Springer-Verlag, New York, 2004).
[8] H.-J. Stöckmann, *Quantum Chaos* (Cambridge University Press, Cambridge, UK, 1999).
[9] N. Chernov and R. Markarian, Math. Surv. Monogr. **127**, 207 (2006).
[10] E. Gutkin and N. Haydn, Ergod. Theory Dyn. Syst. **17**, 849 (1997).
[11] S. Kerckoff, H. Masur, and J. Smillie, Ann. Math. **124**, 293 (1986).
[12] E. Gutkin, J. Stat. Phys. **83**, 7 (1996).
[13] G. Casati and T. Prosen, Phys. Rev. Lett. **83**, 4729 (1999).
[14] P. Bellomo and T. Uzer, Phys. Rev. A **51**, 1669 (1995).
[15] E. J. Heller, Phys. Rev. Lett. **53**, 1515 (1984).
[16] S. Tabachnikov, Stud. Math. **30**, 119 (2005).
[17] P. J. Richens and M. V. Berry, Physica D **2**, 495 (1981).
[18] M. V. Berry and M. Wilkinson, Proc. R. Soc. London, Ser. A **392**, 15 (1984).
[19] E. B. Bogomolny, U. Gerland, and C. Schmit, Phys. Rev. E **59**, R1315 (1999).
[20] T. Gorin, J. Phys. A **34**, 8281 (2001).
[21] E. Bogomolny and C. Schmit, Phys. Rev. Lett. **92**, 244102 (2004).
[22] C. H. Lewenkopf, Phys. Rev. A **42**, 2431 (1990).
[23] P. Bellomo, Int. J. Bifurcation Chaos Appl. Sci. Eng. **5**, 1599 (1995).
[24] H. Ch. Schachner and G. M. Obermair, Z. Phys. B: Condens. Matter **95**, 113 (1994).
[25] A. G. Miltenburg and Th. W. Ruijgrok, Physica A **210**, 476 (1994).
[26] J. L. Varona, Cent. Eur. J. Math. **4**, 319 (2006).
[27] D. D. de Menezes, M. Jar e Silva, and F. M. de Aguiar, Chaos **17**, 023116 (2007).
[28] B. Dietz, T. Friedrich, M. Miski-Oglu, A. Richter, and F. Schäfer, Phys. Rev. E **75**, 035203(R) (2007).
[29] M. L. Mehta, *Random Matrices*, 3rd ed. (Elsevier, Amsterdam, 2004).
[30] G. Casati and T. Prosen (unpublished).
[31] T. Gorin and J. Wiersig, Phys. Rev. E **68**, 065205(R) (2003).